Thermodynamic and Kinetic Aspects of Coassembly of PEO–PMAA Block Copolymer and DPCl Surfactants into Ordered Nanoparticles in Aqueous Solutions Studied by ITC, NMR, and Time-Resol...

ARTICLE *in* MACROMOLECULES · MARCH 2013

Impact Factor: 5.8 · DOI: 10.1021/ma302503w

Macromolecules

Article

pubs.acs.org/Macromolecules

Thermodynamic and Kinetic Aspects of Coassembly of PEO–PMAA Block Copolymer and DPCl Surfactants into Ordered Nanoparticles in Aqueous Solutions Studied by ITC, NMR, and Time-Resolved SAXS Techniques

Mariusz Uchman,*[,†] Michael Gradzielski,[§] Borislav Angelov,[∥] Zdenek Tošner,[‡] Joongseok Oh,[⊥] Taihyun Chang,[⊥] Miroslav Štěpánek,[†] and Karel Procházka[†]

[†]Department of Physical and Macromolecular Chemistry and [‡]NMR Laboratory, Faculty of Science, Charles University in Prague, Hlavova 2030, 128 40 Prague 2, Czech Republic

[§]Stranski Laboratorium für Physikalische und Theoretische Chemie, Technische Universität Berlin, Straβe des 17. Juni 124, 10623 Berlin, Germany

[∥]Institute of Macromolecular Chemistry, Academy of Sciences of the Czech Republic, Heyrovský Square 2, 16206 Prague 6, Czech Republic

[⊥]Department of Chemistry and Division of Advance Materials Science, Pohang University of Science and Technology (POSTECH), Pohang 790-784, Korea

Supporting Information

ABSTRACT: The electrostatic coassembly of a block copolymer polyelectrolyte poly(ethylene oxide-*block*-poly(methacrylic acid), PEO_{705}–$PMAA_{476}$, and oppositely charged surfactant, *N*-dodecylpyridinium chloride (DPCl), has been investigated by a combination of isothermal titration calorimetry (ITC), spin-echo NMR spectroscopy, and time-resolved SAXS measurements. The study (i) confirms the conclusions drawn from our earlier study [*Macromolecules* **2012**, *45*, 6474] by scattering and microscopy techniques (i.e., the ITC curves can be interpreted using arguments consistent with conclusions of the earlier study) and (ii) yields new insight into the thermodynamic and kinetic behavior of the self-assembling system. The most important finding obtained by stopped-flow time-resolved SAXS measurements concerns the surprisingly high rate of processes of creation of structurally ordered cores of self-assembled surfactant–polyelectrolyte nanoparticles (<50 ms).

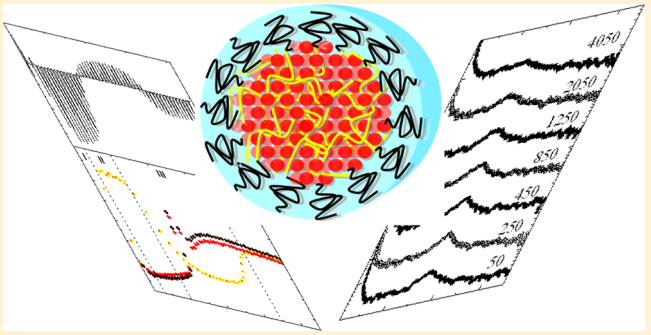

INTRODUCTION

Self-assembled polymeric nanoparticles and nanostructured materials find a number of applications in everyday life of human society. An important class of these materials are the self-assemblies formed as a result of electrostatic interactions. The terms like interpolyelectrolyte complexes (IPEC), block ionomer complexes (BIC), complex coacervate core micelles (C3Ms), and complex polyions have been used in recent years to describe electrostatic complexation between oppositely charged high-molar-mass species. Since the pioneering work of Kataoka and Kabanov on IPEC,[1,2] this subject has been attracting great interest of many research groups due, in part, to the curiosity-driven fundamental research and to promising potential applications of such formulations in, e.g., cosmetics, food technology, and drug delivery.[3−10] The considerable theoretical and experimental effort of researchers resulted in hundreds of papers published on this subject, so it is futile to try to list all relevant articles and it is why we included only a limited number of review papers that appeared recently and are relevant for this study.[3−10]

The formation of electrostatic complexes involves interplay of electrostatic and hydrophobic interactions which control the coassembly of polyelectrolyte–surfactant (PE–S) complexes. Hence, a targeted tuning of molecular characteristics like molar mass, charge density, backbone rigidity, and degree of branching of the polyelectrolyte as well as the length of the aliphatic tail, polarity of the headgroup, and different surfactant architectures (single, double, triple tail) allows one to design and prepare materials with required properties.[10−19] Because the entropy increase due to release of small counterions in bulk solution is the main driving force of the process, the ionic strength of the solution has a very important effect on the

Received: December 5, 2012
Revised: February 26, 2013

   dx.doi.org/10.1021/ma302503w | *Macromolecules* XXXX, XXX, XXX–XXX

complex formation.[8] As the increasing salt concentration screens electrostatic interactions between the polyelectrolyte and surfactant, it appreciably weakens the driving force and slows down the formation of structured assemblies.[20−25] However, while the structures formed fast under the action of a strong driving force are usually kinetically frozen non-equilibrium systems, those formed slowly under screened interactions are often better ordered because the "plasticizing effect" due to solubilization of both positive and negative ions in insoluble domains relaxes the system and enables some exchange of chains between nanoparticles, which leads to a better equilibration during the aging of the system. Experimental proof of the plasticizing effect of ions was provided, e.g., by Pergushov et al.[10,11] and that of better ordering of formed structures by Mironov et al. in the system of poly(diallyldimethylammonium chloride) gel and sodium dodecylbenzenesulfonate (PDADMACl gel−SDBS) complexes.[17]

This article is the second part of a series of papers devoted to the electrostatic coassembly of a high molar mass block copolymer polyelectrolyte, poly(ethylene oxide-*block*-poly(methacrylic acid), PEO_{705}−$PMAA_{476}$ (molar mass 72 kg mol^{-1}), and oppositely charged surfactant, *N*-dodecylpyridinium chloride, DPCl. In the first article, we have reported the formation of core−shell nanostructures with ordered cores containing the crystal-like arrangement of surfactants micelles electrostaticly bound to PMAA blocks.[18] We believe that the high molar mass is a prerequisite for the observed behavior because, e.g., Kabanov et al., who studied a fairly low molar mass sample, did not mention any ordering of core-forming units.[12] Basic behavior of the system and the most important structural characteristics of associates have been investigated by a combination of scattering and microscopy techniques, and the results have already been published in the first report of this series.[18] This paper presents new data that (i) support the conclusions drawn from the previous article and (ii) broaden the knowledge on the association process and understanding the nature of associates. This time we focused on the thermodynamics (isothermal calorimetry titrations, ITC) and kinetics of the self-assembly (time-resolved SAXS measurements) of oppositely charged species and further on the influence of salt concentration and the effect of PEO block on the complexes formation.

EXPERIMENTAL SECTION

Materials. Poly(ethylene oxide)-*block*-poly(methacrylic acid), PEO_{705}−$PMAA_{476}$, M_w/M_n = 1.5, was purchased form Polymer Source, Inc., Dorval, Quebec, Canada. The copolymer was used as received, but because it contains a non-negligible content of relatively low molar mass PEO admixtures, it was first characterized by SEC chromatography. *N*-Dodecylpyridinium chloride hydrate (98%), DPCl, was a product of Aldrich. Deuterium oxide (99.95% D, Eurorad, Germany) was used instead of water in solutions for NMR spectroscopy. Sodium tetraborate, (p.a., ≥99%) was purchased from Fluka and dissolved in water taken from a Millipore system; final buffer concentrations were 50, 10, and 1 mM.

Isothermal Titration Calorimetry (ITC). ITC measurements were performed with a Nano ITC isothermal titration calorimeter (TA Instruments−Waters LLC, New Castle, DE). The measurement was carried out at 25 °C in a 1 mL Hastelloy C sample cell connected to a 250 μL syringe. The syringe needle was equipped with a flattened, twisted paddle at the tip, which ensured continuous mixing of the solutions in the cell rotating at 200 rpm. Titrations were carried out by consecutive 5 μL injections of an aqueous 100 mM DPCl in 1, 10, and 50 mM sodium tetraborate solution from the syringe into the sample cell containing an aqueous 1 g L^{-1} (0.014 mM) PEO_{705}−$PMAA_{476}$ block copolymer in 1, 10, and 50 mM sodium tetraborate solution. A total of 50 consecutive injections were performed. The delay between two consecutive injections was 400 or 900 s. The concentration changes due to injections have been taken into account when analyzing experimental data by the NanoAnalyze software.

Scheme 1. Chemical Structures of Diblock Copolymer and Surfactant Used in This Study: PEO_{705}−$PMAA_{476}$ and *N*-Dodecylpyridinium Chloride[a]**

DPCl

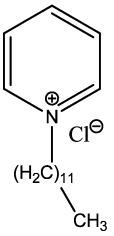

PEO_{705}-$PMAA_{476}$

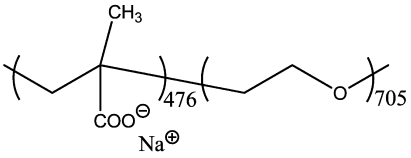

[a]The subscripts denote the degree of polymerization given by the producer.

Nuclear Magnetic Resonance Spectroscopy (NMR). The ^1H NMR data were recorded on Bruker Avance III 600 MHz spectrometer at 25 °C. The two-dimensional ^1H NMR NOESY spectra were measured with the mixing times 50, 150, and 300 ms. The one-dimensional selective NOE experiments on samples with 50 mM sodium tetraborate and PEO_{705}-*b*-$PMAA_{476}$:DPCl ratios of 1:1 and 1:2 were also performed.

Measurements of translational diffusion coefficients were performed with the double stimulated echo experiment with bipolar pulse field gradients described by Jerschow et al.[26] The pulse sequence has been optimized to suppress flow and convection artifacts as well as eddy current effects. The use of bipolar gradients removes possible modulation of the intensity decay curves by chemical exchange occurring between the sites with different chemical shifts.[27] The gradients were 1 ms long with 16 different linearly spaced amplitudes spanning the range 0−60 G cm^{-1}, and the diffusion time was 1 s. The calibration was done using a standard sample of 1% H_2O in D_2O (doped with $GdCl_3$), for which the value of the HDO diffusion coefficient at 25 °C is 1.9×10^{-9} m^2 s^{-1}.[28] All data processing and fitting of the diffusion coefficients has been done using the spectrometer software (Topspin 2.1, Bruker).

Time-Resolved Small-Angle X-ray Scattering (SAXS). Small-angle X-ray scattering measurements were done at the ID02 beamline at the European Synchrotron Radiation Facility in Grenoble, France. The detector was a high-sensitivity CCD FReLoN 4 M detector, the area of which was divided into 512 × 512 pixels after 4 × 4 pixels binning. This binning slowed the detector readout time to 190 ms. The X-ray wavelength was 0.1 nm, the beam size was 350 × 270 μm^2, and the accessible *q*-range was from 0.07 to 3.2 nm^{-1}. The mixing of the surfactant and the polymer solutions was done by a stopped flow apparatus (SFM-400, Bio-Logic, Claix, France) equipped with four motorized syringes interconnected through three mixers. The scattering cell of the stopped flow apparatus was made from quartz capillary (1.5 mm diameter, wall thickness 10 μm) and connected to the exit of the mixer cell. The mixing time of the two components in the cell is 3.3 ms, according to the calibration procedure described previously.[29] The SAXS measurement (data collection) started 40 ms and finished 50 ms after the end of the mixing procedure; i.e., the incident and transmitted beam intensities were recorded simultaneously for 10 ms. Silver behenate was used for the *q*-range calibration and glassy carbon for the intensity normalization. After the data acquisition, the obtained 2D images were integrated into 1D scattering curves by means of the SAXS Utilities software developed especially for the ID02 beamline. The background scattering, coming from the quartz capillary and the solvent, was measured and subtracted using

dx.doi.org/10.1021/ma302503w | Macromolecules XXXX, XXX, XXX−XXX

conventional procedures taking into account the transmission of the various measurements. The use of one and the same stop flow capillary during the measurements with and without solvent allowed for a very precise subtraction of the background.

Chromatography. GPC analysis of PEO_{705}–$PMAA_{476}$ was carried out in aqueous phase using two TSK gel PW_{XL} columns (hydroxylated polymethacrylate, 300 mm × 7.8 mm i.d., 13 μm particle size). The eluent was aqueous solution of 0.1 M Na_2HPO_4 at pH 9.4. A refractive index detector in Viscotek TDA 302 was used to record the chromatogram. Concentration of injection samples was 0.5 wt %, and the injection loop volume was 100 μL. The temperature of the column was controlled by a column oven. To estimate the amount of the PEO homopolymer in the commercial sample of PEO_{705}–$PMAA_{476}$, the dn/dc values of PEO and PMAA in water were found in the literature as 0.135 and 0.142, respectively.[30]

RESULTS AND DISCUSSION

As already mentioned, the copolymer sample studied in this (and also in the previous) paper was used as supplied by the producer. According to the chromatogram provided by the producer (available at www.polymersource.com), it is obvious that it contains a non-negligible content of short free PEO chains. Therefore, we decided to perform an advanced SEC analysis. Even though neutral PEO chains are not expected to interact appreciably with cationic surfactant (as it was also proven by ITC—see later), information on the content of free PEO chains is important because it may influence the calculation of the length of soluble blocks in the copolymer, based on experimentally measured characteristics provided by the producer.

Chromatographic analysis of a PEO_{705}–$PMAA_{476}$ sample was performed at three temperatures 30, 50, and 80 °C in 0.1 M Na_2HPO_4, at pH 9.4, and the peaks of low molar mass PEO pollutants were always compared with elution curves of PEO standards. It was found (for details see Supporting Information) that at low temperatures PEO chains separate according to SEC mechanism, while at 80 °C, PEO chains appear to interact strongly with the GPC stationary phase. Their elution volumes of PEO shift to higher values than that of low molar mass solvent and do not almost depend on molar mass. The peak of PEO admixtures is well separated from the copolymer peak, and therefore the evaluation of the overall content of free PEO was performed at 80 °C (Figure 1). The analysis of chromatograms (supported by MALDI-TOF data) indicates that the commercial sample contains ca. 24 wt % of low molar mass PEO (M_w ca. 1–3 kDa).

It is evident that the content of low molar mass PEO admixtures is quite high, which means that the length of PEO block is somewhat shorter than that based on information by the producer, but it is still sufficiently long to stabilize the complex copolymer–surfactant nanoparticles in the solution. Neutral PEO does not interact with cationic surfactant (see later). Therefore, the presence of free PEO chains does not affect the association process. As the molar mass of PEO admixtures is low, the presence of short free chains does not almost influence scattering data, and last, but not least, PEO chains are almost invisible in microscopy imaging. Thus, we can summarize that, even though the sample contains PEO homopolymer admixtures, their presence should neither invalidate the study, nor appreciably modify the previous results, nor affect general conclusions drawn from both communications.

The study was performed in alkaline buffer at high pH, when carboxylic groups are dissociated and no specific interaction

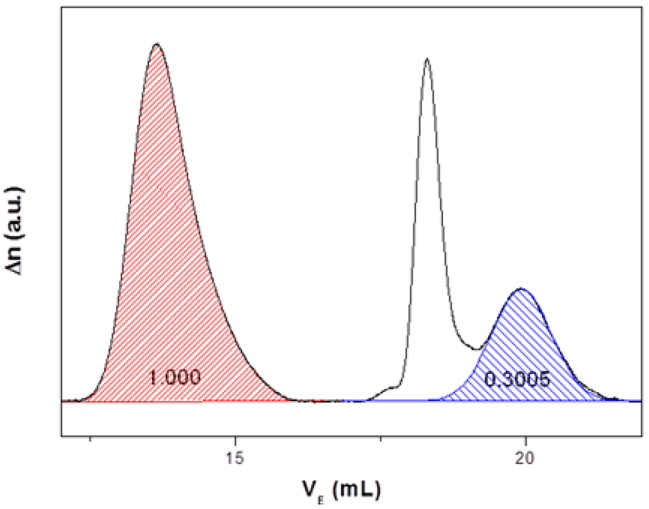

Figure 1. Aqueous GPC chromatogram of PEO_{705}–$PMAA_{476}$ using 0.1 M Na_2HPO_4 as eluent. Areas of the elution peaks of PEO_{705}–$PMAA_{476}$ (red) and PEO homopolymer (blue) at 80 °C. White peak corresponds to the elution of the low molar mass solvent. Remark: because of interaction of PEO with the stationary phase, the elution volume of PEO exceeds that of low molar mass solvent.

between PMMA and PEO units takes place.[31,32] The investigation of the self-assembling behavior of the system and basic structural characterization of aggregates have been done by a combination of static and dynamic light scattering, SANS, and SAXS together with microscopy techniques, and the results have been published recently.[18] In this article, we focus on the thermodynamics and kinetics of the process. For the sake of an easy and smooth discussion, let us briefly outline the most important facts established earlier: (i) At low surfactant-to-polyelectrolyte ratios (Z less than ca. 0.6), large aggregates formed by swollen copolymer chains, PMAA blocks of which are decorated and interconnected by surfactant micelles. (ii) At Z higher than 0.6, compact spherical aggregates with dense polyelectrolyte–surfactant complex containing cores start to form, and they coexist in the solution with swollen aggregates. The cores contain highly ordered (crystalline-like) assembly of surfactant micelles electrostatically bound to PMAA chains. (iii) At Z ca. 1, all PEO_{705}–$PMAA_{476}$ chains are engaged in the formation of core–shell aggregates, and at higher Z, free excess surfactant micelles coexist with polymer–surfactant nanoparticles.

Micellization of DPCl in Sodium Tetraborate. As already mentioned, the study has been performed at high pH in a tetraborate buffer. The micellization of DPCl has been studied in several aqueous buffers by ITC,[33] surface tension, and conductivity methods,[34] but no data on its behavior in sodium tetraborate buffer are available. It is why we performed ITC measurement for the pure surfactant first (Figure S2a,b). The cmc values determined in this study were as follows: 9.8, 15.4, 16.5, and 18.3 mM in 50, 10, 1 mM buffer, and pure water, respectively. The cmc value for DPCl in pure water at 25 °C is in good agreement with data reported earlier, e.g., with a value 17.5 mM by ITC[33] and 17.8 mM obtained by surface tension measurement at 20 °C.[34] Enthalpies of micellization range from 2.7 kJ mol^{-1} for DPCl in 50 mM buffer to 1.7 kJ mol^{-1} for DPCl in pure water. For more details on the thermodynamics of DPCl micellization and influence of the

dx.doi.org/10.1021/ma302503w | Macromolecules XXXX, XXX, XXX–XXX

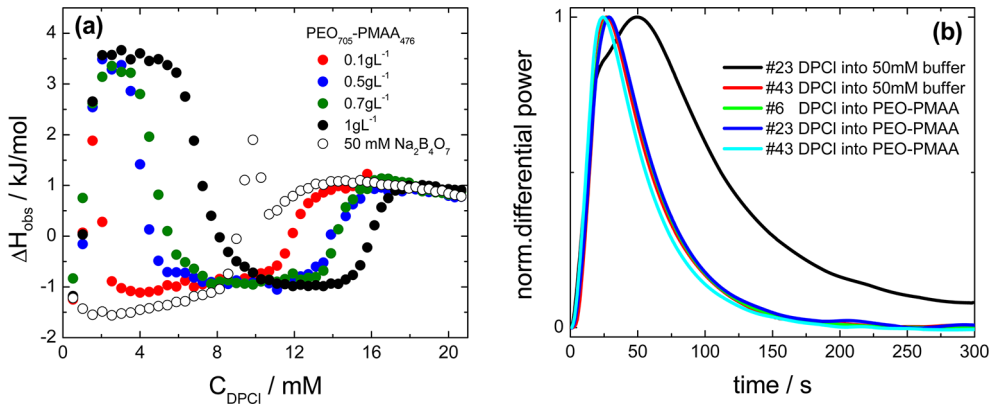

Figure 2. (a) Enthalpy curves for titrating of DPCl into PEO_{705}–$PMAA_{476}$ aqueous solutions at different PEO_{705}–$PMAA_{476}$ concentrations and constant salt concentration (50 mM $Na_2B_4O_7$). (b) Normalized differential power as a function of the time for different injection of 100 mM DPCl into 50 mM buffer and 1 g L^{-1} PEO_{705}–$PMAA_{476}$.

rate of stirring on transient peak (Figure S3a,b) see the Supporting Information.[35−46]

Comicellization of DPCl with PEO_{705}–$PMAA_{476}$. The formation of structured nanoparticles in the solution due to interaction of PEO_{705}–$PMAA_{476}$ with DPCl is a complicated process not only from the thermodynamic but also from the kinetic points of view, and thermal effects accompanying the appearance of individual structures are both exo- and endothermic. The analysis of nonmonotonous ITC curves requires great care, but it simultaneously offers a possibility to follow structural transitions in the system. The curves in Figure 2a depict differential heats obtained by integration of raw data during titrations of DPCl into PEO_{705}–$PMAA_{476}$ buffered solutions with different copolymer concentrations. All measured curves clearly show that with increasing content of DPCl the system undergoes three distinct stages which differ in signs of measured thermal effects. The very first additions of DPCl (full circles) are accompanied by strong endothermic effects which steeply grow and soon reach a maximum. Then they almost level off in a certain DPCl concentration region starting at the surfactant-to-polymer ratio, Z ca. 0.3, i.e., at significantly lower Z than 1. As compared with the demicellization of pure surfactant (empty circles), it is evident that the binding of DPCl to polymer chains starts well below the cmc in a given buffer. Positive enthalpy suggests that a significant increase in entropy is the decisive driving force of the observed association process. Using the knowledge gained in our previous study by scattering and microscopy methods,[18] we can describe the first stage as the formation of large swollen polymer–surfactant aggregates with DPCl micelles electrostatically bound to PMAA chains. The main driving force is an appreciable increase in translation entropy of small ions released in bulk solution after binding the surfactant to PMAA chains, and the positive enthalpy is mainly due to changes in water structure after the solvation of Cl^- ions (the so-called "water structure breaking effect by large ions").[47]

When the amount of added surfactant approaches $Z = 1$, the curves change quite fast, albeit smoothly, and further additions of DPCl generate exothermic heat effects. It is worth mentioning that the measured curves remain almost constant in a broad range of Z ratios. In this region, the light and neutron scattering measurements proved the formation of compact nanoparticles with cores formed by insoluble polyelectrolyte–surfactant complex and water-soluble PEO shells that stabilize the particles in the solution. The SAXS measurement indicates that the surfactant micelles in insoluble cores are highly ordered. Combining the pieces of information obtained earlier[18] with ITC data, we can conclude that the decrease in the Gibbs function and the consequent driving force is a combination of the entropy-favored release of small ions and suppression of unfavorable interactions of insoluble complex with water molecules. The combined enthalpy effect reflects several types of interactions. We assume that changes in water structure, i.e., the promotion of the structure in the concentrated PEO shell,[48] contribute significantly to the exothermic effect. However, one more contribution, which is responsible for a long constant exothermic region covering a broad range of Z, has to be taken into account. This effect can be explained with help of light scattering, SANS,[18] and NMR data (see later): Both methods show that at $Z > 1$ a minor fraction of surfactant solubilizes (together with a corresponding amount of counterions) in complex cores which slightly swell. A major fraction of free DPCl remain in the solution and coexist with polymer–surfactant nanoparticles, which indicates that chemical potentials of the surfactant in both media are equal. The spin-echo NMR measurement of diffusion coefficients suggests that at $Z > 3$ all newly added DPCl remains in the bulk solvent (see later). The exothermic region of enthalpy curves for polyelectrolyte–surfactant systems, which broadens with decreasing copolymer concentration, is observed because at low PEO_{705}–$PMAA_{476}$ concentration, the compact core–shell particles start to form at DPCl concentrations appreciably lower than the cmc and the dissociation of a part of added DPCl micelles at $Z > 1$ which remain in the bulk solution below cmc as unimers generates the exothermic contribution to the observed heat effect. The lower is the PEO_{705}–$PMAA_{476}$ concentration, the lower is the concentration when compact core–shell particles start to form as compared with cmc of the surfactant, and the longer is the constant exothermic plateau at the Z scale. This conclusion is confirmed by ITC because at high Z all curves converge to endothermic values obtained by the ITC measurement for pure surfactant above the cmc, when the dilution of micelles is the only process responsible for the observed heat effect. The second pronounced change of the heat effect (connected with the sign change) to slightly endothermic values is shifted to higher DPCl concentrations as compared with cmc because the surfactant starts to concentrate in the bulk solution only after its non-negligible part has been consumed in the process of polyelectrolyte–surfactant formation; i.e., its steep sigmoidal

dx.doi.org/10.1021/ma302503w | Macromolecules XXXX, XXX, XXX–XXX

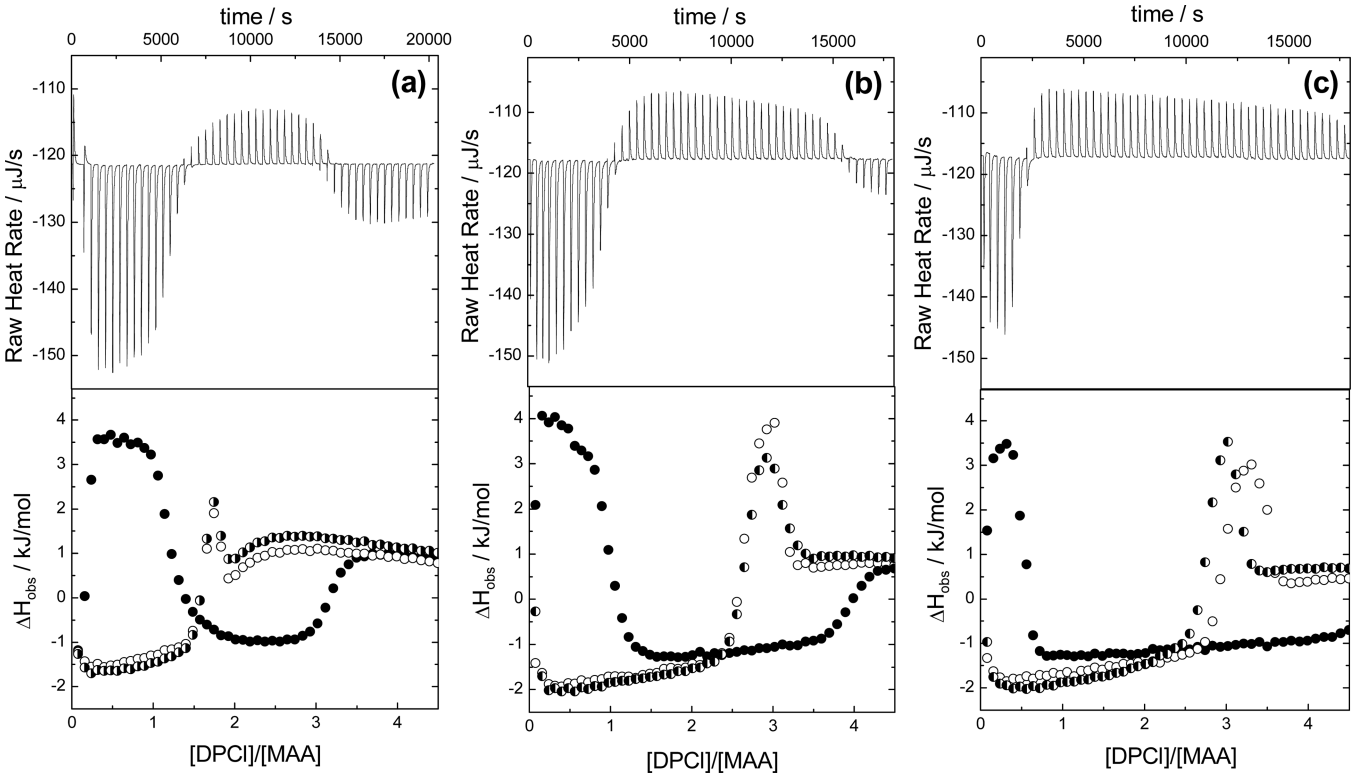

Figure 3. ITC raw data (upper panel) and enthalpy curves (lower panel) of titrating DPCl into (●) 1 g L^{-1} PEO_{705}–$PMAA_{476}$, (○) pure $Na_2B_4O_7$ buffer, and (◐) 1 g L^{-1} PEO_{943} at different $Na_2B_4O_7$ concentration: (a) 50 mM, (b) 10 mM, and (c) 1 mM.

part shifts to higher DPCl concentrations with increasing PEO_{705}–$PMAA_{476}$ concentration.

The fact that the measured heat effects are large, nevertheless the changes from endo- to exothermic values and vice versa proceed smoothly at the DPCl concentration axis, or at *Z*-axis (even though the measurement has been performed slowly; i.e., individual small additions of DPCl solutions are separated by 900 s), supports the conclusions drawn from the fitting of SANS scattering curves, i.e., that the weight concentrations of individual forms change continuously with *Z* and different types of aggregates coexist in relatively broad *Z* regions.[18]

Figure 2b qualitatively compares the shapes of the ITC signals observed in three different parts of raw data curve for copolymer–surfactant system (copolymer concentration c = 1 g L^{-1}) with shapes of regular and transient peaks for of DPCl micelles. It is obvious that the decay rates of transient peaks in pure surfactant micelles (in fact, not only the return to the baseline but also a delayed built up; #23 addition of DPCl into 50 mM buffer) are appreciably slower than those of "regular" peaks and also slower than those observed in surfactant–polymer system. Hence, it is evident that the transient peaks reflex enthalpy effects of different processes than the formation of regular micelles. It is also worth mentioning that the calorimetric response in polymer containing mixtures is fast (comparable with that in pure surfactant systems), which indicates a high rate of involved association processes (see later; the time-resolved SAXS measurements).

In the next part, we studied the effect of ionic strength on the association processes and investigated the role of the water-soluble PEO block. Figure 3 shows raw ITC data (the upper part) and integrated differential heats (lower part) produced during the titration of PEO_{705}–$PMAA_{476}$ solutions by DPCl micelles in $Na_2B_4O_7$ buffers of different concentrations: c = 50 mM (a), 10 mM (b), and 1 mM (c). Full circles depict the titration of the copolymer solution, and empty circles show the demicellization of DPCl in pure buffer for comparison. We were also interested if the PEO homopolymer interacts with DPCl, and therefore we performed a titration into the PEO containing buffer (half-filled circles).

The curve for the surfactant–polymer system in a high ionic strength solution (50 mM buffer) when the electrostatic forces are efficiently screened is in fact one of the already discussed curves from Figure 2. The most important observation at the high ionic strength is that the open and half-filled circles almost overlap, which means that PEO does not interact with surfactant micelles and does not affect their micellization.

At an intermediate ionic strength (10 mM buffer), the cmc of the copolymer increases as expected on the basis of experimental and theoretical studies of ionic surfactant systems.[49] The presence of PEO does not almost affect the surfactant micellization, except the transient part close to the cmc. As the cmc value is higher, the constant exothermic part reflecting the dissociation of excess free surfactant micelles not participating in formation of complex nanoparticles is longer, simply because higher amounts of DPCl are needed in bulk solution to reach the cmc.

At a low ionic strength (1 mM buffer), we observe further increase in cmc and more pronounced differences between transient parts of surfactant demicellization curves in the presence and absence of PEO in the buffer solution. However, the most obvious effects are faster decrease of the first sigmoidal part of the curve for the polyelectrolyte–surfactant system and its shift and to *Z* values appreciably lower than 1 due to increased effect of strong nonscreened electrostatic interactions.

dx.doi.org/10.1021/ma302503w | *Macromolecules* XXXX, XXX, XXX–XXX

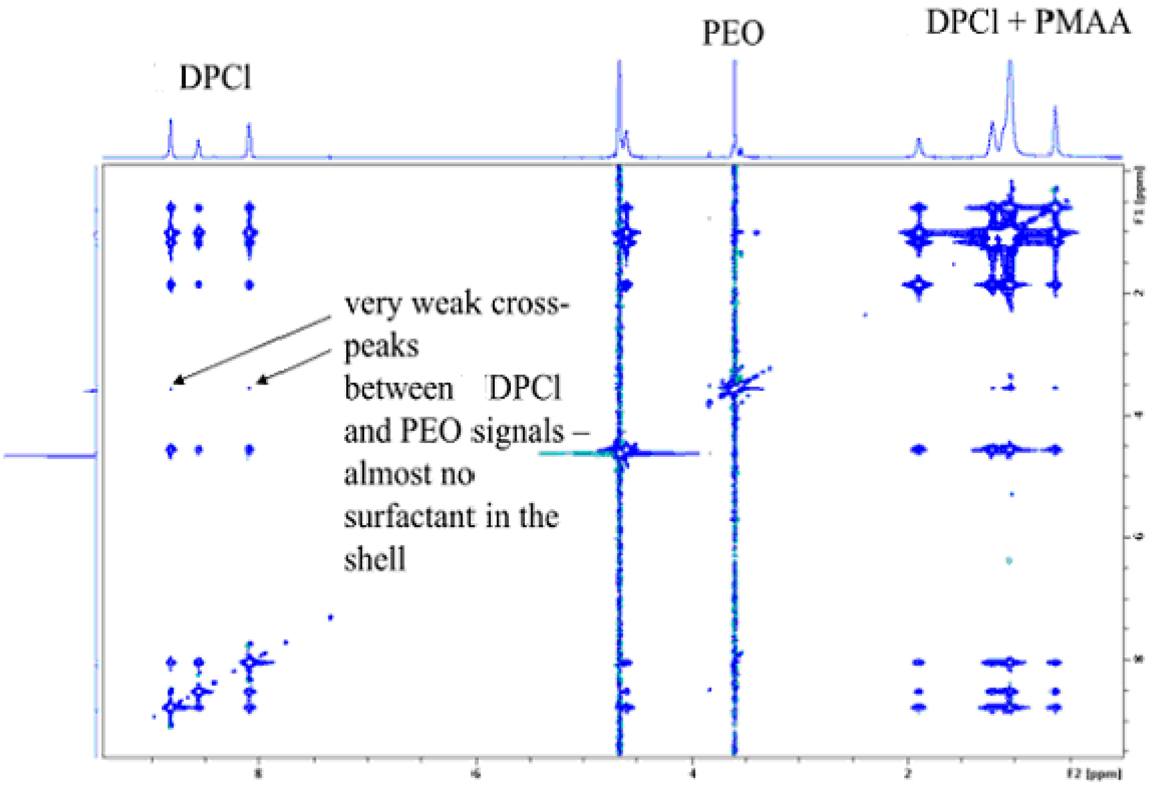

Figure 4. Two-dimensional ^{1}H NMR NOESY spectra of PEO_{705}–$PMAA_{476}$/DPCl complex at Z = 2 in 50 mM $Na_2B_4O_7$ in D_2O.

To summarize and close the ITC part, we can say that the isothermal titration calorimetry study provides deep insight into the thermodynamics of complex self-assembly processes, which besides rich interplay of polymer interactions with other components include also the reorganization of counterions and solvent molecules (particularly in aqueous media). The observed changes can be explained using arguments that are consistent with results of our earlier study.[18] The results of DPCl titration into PEO-containing buffer show that the PEO–surfactant interaction is negligible, and hence we can conclude that the presence of free PEO chains in the studied sample does not appreciably affect the electrostatic surfactant–copolymer self-assembly.

In some cases way of mixing (surfactant into polymer or polymer into surfactant) is very important and leads to new information about equilibrium state of the complexes.[36] This is why we performed inverse ITC experiments, i.e., add the copolymer solution to DPCl solutions above (Figure S4a) and below (Figure S4b) cmc of the surfactant. The comparison of ITC curves indicates that the self-assembly processes is reversible (for detailed discussion on inverse ITC titration see the Supporting Information).

2D ^{1}H NMR NOESY Study of the Supramolecular Structure of the PE–S Complexes. To get supplementary pieces of information on the microstructure of the PE–S complexes, we performed 2D ^{1}H NMR NOESY experiments aimed at ascertaining which protons in the system are close to each other (<5 Å) and can mutually interact. Figure 4 shows reasonably well-pronounced cross-correlation peaks between proton signals from DPCl and those from PMAA block for nanoparticles prepared at Z = 2, indicating the formation of mixed cores containing the surfactant–polyelectrolyte complex. The signals of the stabilizing shell-forming PEO block (3.73 ppm) show very weak cross-correlation peaks with DPCl (8.18 and 8.95 ppm), indicating that surfactant molecules do not interact significantly with PEO block which was proved also by ITC experiments. Only a small number of DPCl micelles located in the subsurface layer of the core and a small number of PEO units in the innermost part of the shell are sufficiently close to each other and interact which gives rise to the observed weak cross-correlation peaks

NMR Study of Self-Diffusion. Figure 5 shows the dependence of the diffusion coefficient of DPCl measured by the spin-echo NMR on its concentration in pure 50 mM sodium tetraborate D_2O (empty square) and that of complex nanoparticles on the DPCl-to-PEO_{705}-$PMAA_{476}$ molar charge ratio, Z (filled square), in the same buffer. The measured

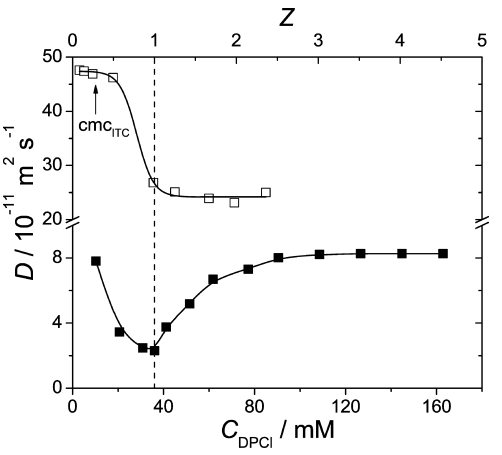

Figure 5. Diffusion coefficient of DPCl in D_2O solution of 50 mM $Na_2B_4O_7$ buffer (empty square) and in PEO_{705}–$PMAA_{476}$ copolymer complexes as a function of Z in the same buffer (filled square).

dx.doi.org/10.1021/ma302503w | Macromolecules XXXX, XXX, XXX–XXX

diffusion coefficient of pure DPCl decreases steeply in the cmc region due to formation of surfactant micelles. The value obtained above the cmc in the buffer used is fairly similar to that reported by Sandt et al. in water at 23 °C, which is 18 × 10^{-11} m^2 s^{-1}.[50] As indicated in Figure 5, the cmc determined by ITC differs form that obtained by NMR; however, we have to keep in mind that different solvents (D_2O and H_2O) have been used in both experiments, and of course, the sensitivity of both methods to the presence of large particles and to cmc is different. The dependence of the diffusion coefficient on Z measured in surfactant−polyelectrolyte copolymer mixtures (filled squares) is nonmonotonous. Diffusion coefficients decrease in the concentration Z range 0 to 1 (which corresponds to concentrations 0 to 38 mM) due to the formation of aggregates. At higher Z, they increase again because the concentration of small free surfactant molecules and later that of surfactant micelles (above cmc), which coexist together with large polyelectrolyte−surfactant complex micelles, increases. At $Z > 3$, almost all surfactant micelles newly added to the solution stay outside polymer−surfactant particles, and their number concentrations exceeds that of large particles. For a proper understanding of the shape of the measured curve and for comparison of values measured by NMR and by dynamic light scattering, it is necessary to keep in mind that NMR yields the number-average data while DLS provides Z-averages which are strongly affected by large scatterers. It explains why the NMR-based values increase at $Z > 1$ and level off at $Z > 3$ and why they differ from those obtained by DLS. In contrast to DLS data, they reflect the growing concentration of relatively small free DPCl micelles at large Z. The spin-echo NMR study thus unambiguously confirms our indirect conclusion drawn from the analysis of SANS curves concerning the coexistence of compact polyelectrolyte−surfactant nanoparticles with small free surfactant micelles at high Z.[18]

Time-Resolved SAXS Measurements. Proper understanding of the behavior of self-assembled polymer systems requires a good knowledge of the mechanism and kinetics of nanoparticle formation. The main reason is the following: The underlying association processes and their different pathways quite often involve high energetic barriers[51−54] which means that various kinetically trapped nanostructures can be obtained according to applied preparation procedures and conditions.[55] Numerous experimental observations indicate that in the case of direct mixing of components the rate of mixing and how it is performed strongly affect the shape, size, and size distribution of the resulting associates.[56] While the formation of surfactant micelles proceeds usually on the millisecond time scale, association processes in polymer systems are considerably slower.[57] In the latter systems, the measured rates of relaxation processes depend strongly on solvent selectivity, and the corresponding time constants have been found in the region of seconds to days.[58,59] The studied system is a mixture of polymer chains and surfactant molecules, which (as separate systems) self-assemble on different time scales. As the rate of formation of studied complex structures depends on the pathway how the mutually interacting components of very different sizes get organized and the slowest step limits the overall rate, one would intuitively expect the rate in between those of both constituent systems. Because no data on the rate of formation of PEO_{705}−$PMAA_{476}$ and DPCl complex nanoparticles have been published so far, we addressed this challenging problem by time-resolved SAXS measurements. It should be honestly made clear that neither the measurement nor data interpretation has been straightforward. Measured curves are affected by interaction of the sample with very intense X-ray beam which causes disruption and possible degradation of the complex and manifests itself as a non-negligible "melting" of crystalline cores. However, a high intensity of the beam is necessary because it minimizes the time interval necessary for acquisition of sufficiently high number of photons to secure good data statistics. During this interval the time-resolved data are actually time-averaged, and the used intensity was a result of a compromise between 10 ms time acquisition and 50 ms time increments (which sets up the time resolution of the measurement). To asses (at least partially) the effect of the above-mentioned hassle, the same time-resolved SAXS measurements were performed on a long-time-equilibrated PEO_{705}−$PMAA_{476}$/DPCl system of the same composition because the comparison of measured data helps to understand the role of processes involved.

In our experiment, we monitor the appearance and changes of correlation peaks in the q-region 1.5−2.0 nm^{-1}. In our previous study, we have shown both by SANS and SAXS that peaks in this region appear only in solutions containing the core−shell nanoparticles which form at $Z > 0.6$. They reflect the regular arrangement of surfactant micelles in insoluble cores formed by the polyelectrolyte−surfactant region. Hence, they are typical features of nanoparticles with highly ordered cores, indicate their presence in the system, and can be used for monitoring the kinetics of processes of their formation. The SAXS curves obtained in both experiments are shown in Figure 6. In case of the stopped-flow experiment, the first 10 ms

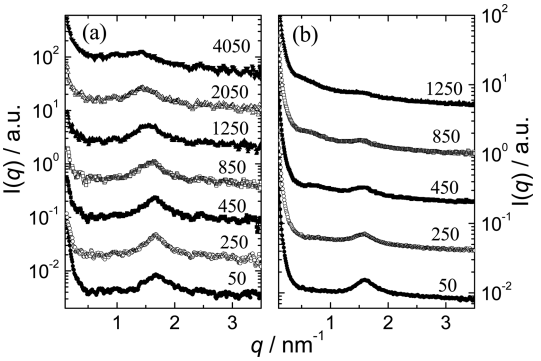

Figure 6. Time-resolved SAXS curves for (a) stopped-flow mixed and (b) equilibrated PEO_{705}−$PMAA_{476}$/DPCl system (Z = 1.08). Numbers above the curves indicate time in milliseconds after opening the X-ray beam shutter. Each curve was recorded for 10 ms.

irradiation started 40 ms after the beginning of the mixing experiment. All other successive 10 ms irradiations are separated by 200 ms; i.e., the second pulse starts 190 ms after the end of the first one, etc. The given values thus indicate real time measured from the beginning of the mixing experiment. Because the samples are intermixed on the time scale of units of ms (typically 3.2 ms), the values roughly correspond also to time intervals elapsed upon a full intermixing of components. The pulse sequence used in case of the premixed and long-time equilibrated sample is exactly the same as the previous one, except that the time zero does not correspond to the start of the mixing experiment, but it is artificially shifted by −50 ms with respect to the end of the first pulse. As explained above, an increase in the scattering intensity and development of well-pronounced correlation peak does

dx.doi.org/10.1021/ma302503w | Macromolecules XXXX, XXX, XXX−XXX

indicate not only the formation of large nanoparticles but also the creation of compact domains with ordered surfactant micelles. Here it should be pointed out that the correlation peak shows up very early, which indicates a surprisingly fast structure buildup. In both experiments, it disappears with time due to degradation of the sample by the X-ray beam and disruption of the ordered structure. The decay of the intensity of the correlation peak is substantially slower in the case of the stopped-flow experiment (cf. scattering data at 1250 ms), which could be a result of competition between late stages of the structure built up and the X-ray-induced sample degradation. Moreover, despite the fact that a homogeneous intermixing of the components in up-to-date stopped flow setups is fast (ca. 2−3 ms), some residual macroscopic motion of the homogeneous mixture in the cell and exchange of PEO_{705}−$PMAA_{476}$/DPCl particles in the irradiated volume, which decreases the effective irradiation time and the "structure melting", cannot be a priori ruled out.

The full width at half-maximum (fwhm) of the correlation peak, γ, and the q value of the maximum, q_{max}, are related to the correlation length of the ordered system of surfactant micelles, ξ, and the characteristic distance between centers of the neighboring micelles, L, respectively, as $\xi = 2/\gamma$ and $L = 2\pi/q_{max}$. Both ξ and L are shown in Figure 7 as functions of time

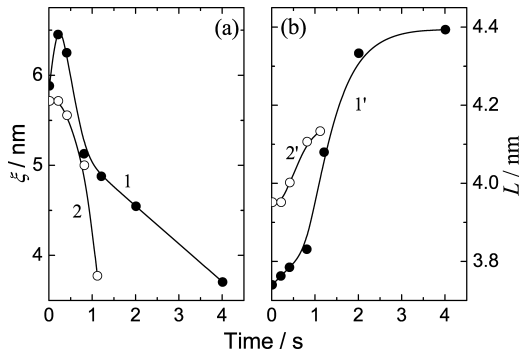

Figure 7. (a) Correlation length and (b) characteristic center-to-center distance for DPCl micelles embedded in the core of PEO_{705}−$PMAA_{476}$/DPCl nanoparticles (Z = 1.08) from the time-resolved SAXS measurements of stopped-flow mixed (curves 1, 1′) and equilibrated (curves 2, 2′) PEO_{705}−$PMAA_{476}$/DPCl system.

for both stop flow and static experiment. For both systems, the correlation length (curves 1, 2) increases and the characteristic distance (curves 1′, 2′) decreases with time as a result of the disruption of the ordered structure due to X-ray irradiation, except for a certain increase of ξ upon mixing (curve 1) which suggests that after the fast first step a slower structure development proceeds in cores of formed PEO_{705}−$PMAA_{476}$/DPCl particles on the time scale of 10^{-1} s. This observation is compatible with our assumption (based on intensity changes of the correlation peaks only) that the late slow steps of the structure buildup and ripening take place and compete with the disruption of the ordered structure by X-ray beam at the time scale of seconds and affect scattering data in the case of the stop flow experiment.

When discussing the stop-flow data, it is of interest to calculate the mean-square distances that the constituents forming the large core/shell structures reach by diffusion and compare them with average distances between free polymer chains and centers of micelles in the solution. The diffusion coefficient obtained by spin-echo NMR measurements for surfactant micelles is 25×10^{-11} m^2 s^{-1}, and that of compact high-molar-mass associates is 2×10^{-11} m^2 s^{-1} (the coefficient of free polymer chains should be of course larger than the latter value—we use that of associates as a lower limit). It means that the mean-square distance that the surfactant micelles and copolymer chains reach by diffusion within 50 ms is 5000 nm and (minimum) 1400 nm, respectively. Average distances between free polymer chains (before micellization) are 50 nm, and those between centers of micelles are 400 nm (based on concentrations and estimated molar masses). It is obvious that the diffusion-limited rate is fast enough, and both the surfactant micelles and polymer chains can incorporate in ordered structures by diffusion within 50 ms and that the observed fast formation of structures with "crystalline-like" cores is a feasible and physically meaningful process.

In summary, the stopped flow measurement proves that the formation of ordered domains is very fast as the correlation peak is observable from the very beginning of the measurement, i.e., ca. 50 ms after the intermixing of components. High intensity of applied X-ray pulses and subsequent disruption of the studied structures hinders accurate measurements and precludes proper analysis of time-dependent curves reflecting structural development of compact cores, but it does not invalidate the conclusion on the high rate of structure development.

CONCLUSIONS

The performed study yields new thermodynamic and kinetic data on the electrostatic self-assembly of PEO_{705}−$PMAA_{476}$ with DPCl in aqueous solutions. Results of newly applied techniques confirm the conclusions concerning the structure of aggregates obtained earlier[18] by scattering and microscopy techniques, provide insight in the behavior of the system from new points of view, and complete the mosaic of our knowledge.

The ITC curves obtained by titrating the buffered PEO_{705}−$PMAA_{476}$ solutions with fairly concentrated DPCl solutions indicate three different self-assembly regimes, which differ in signs of accompanying enthalpy effects depending on the surfactant-to-polyelectrolyte ratio, Z. The measured effects reflect complex processes which, besides the changing surfactant−polyelectrolyte interactions due to formation of self-assembled structures, comprise also changes in water structure and redistribution of counterions. However, the shapes of measured curves can be explained using the arguments consistent with observations and conclusions drawn from our earlier studies concerning the structure of aggregates in different Z regions. Scheme 2 (i) in the region of low Z, the surfactant−polyelectrolyte interaction leads to the formation of micelle-decorated chains. The surfactant-to-polyelectrolyte binding and a subsequent association of DPCl-decorated chains in loose aggregates are detected at DPCl concentrations significantly lower than the cmc of the pure surfactant in a corresponding buffer. The measured enthalpy is positive, which means that the process is driven mainly by the entropy increase due to liberation of small counterions and their escape in bulk solution. (ii) At Z ca. 0.6, compact high molar mass core−shell aggregates with ordered cores start to form. At lower $Z \in 0.6$−1.0, they coexist in equilibrium with loose aggregates and (iii) at high $Z > 1$, with free surfactant molecules or with micelles, depending on the concentration of free excess surfactant (not engaged in formation of complex cores) with respect to the cmc. The enthalpy of formation of compact nanoparticles reflects several

dx.doi.org/10.1021/ma302503w | Macromolecules XXXX, XXX, XXX−XXX

Scheme 2. Schematic Drawing of the Co-assembled Structures in Solution of PEO_{705}−$PMAA_{476}$/DPCl at Different Molar Ratio Z (Based on Results of Both Papers Devoted to the Studied Topic)

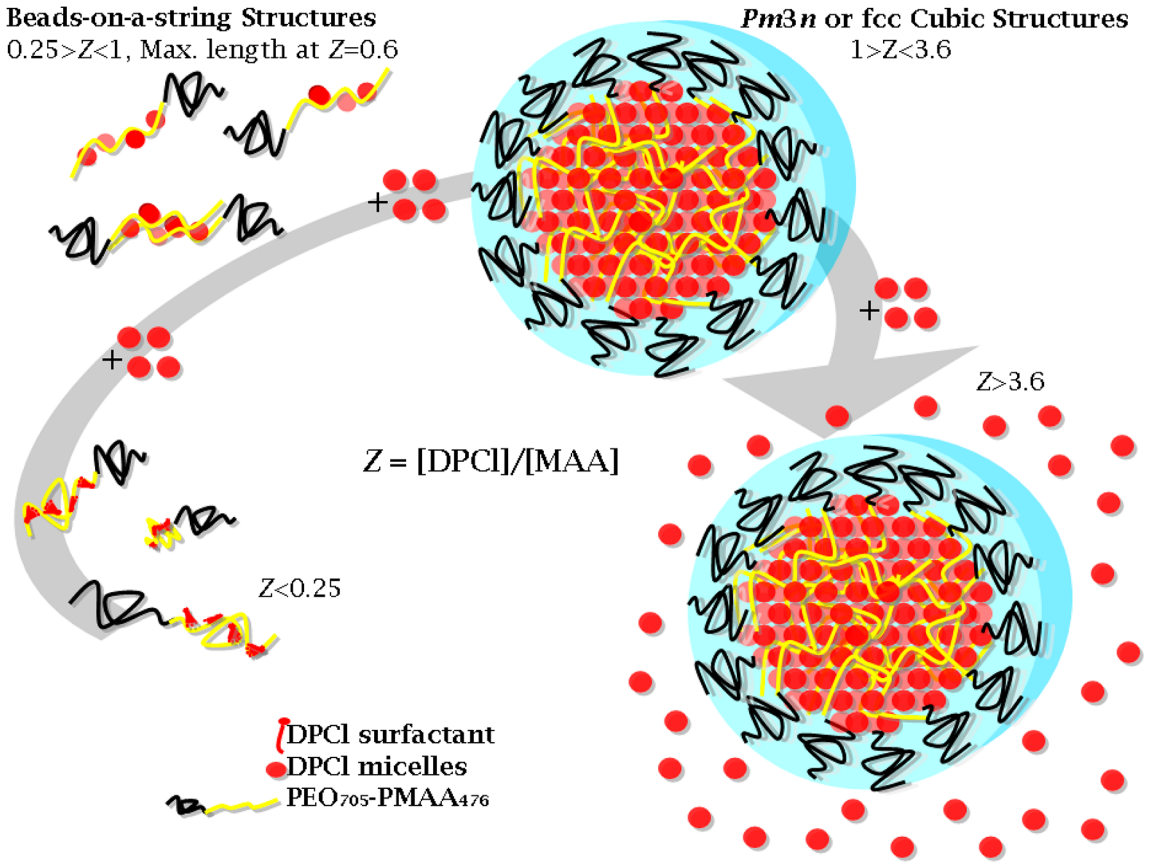

contributions, e.g., the suppression of unfavorable interactions between the insoluble complex and water molecules, changes in water structure, etc. At $Z > 1$, when a significant amount of the surfactant remains in the solution outside large nanoparticles, enthalpy effects accompanying the dissociation of surfactant micelles (when concentration of DPCl outside nanoparticles is lower than the cmc) and/or their dilution above the cmc contribute appreciably to the observed thermal effect.

The spin-echo ^{1}H NMR measurements unambiguously prove our indirect conclusion that we have formulated on the basis of SANS data fitting in our earlier study:[18] i.e., that at high Z, a considerable fraction of DPCl dissolve in the bulk solvent in form of molecules of small micelles depending on the concentration with respect to the cmc. The dependence of the number-average diffusion coefficient (based on the proton signal from DPCl) is not monotonous. At first it decreases, indicating the incorporation of DPCl in large surfactant−polyelectrolyte particles, and then it increases and levels off again at high Z (or DPCl concentration) due to the increasing number of small free (and therefore highly mobile) DPCl species in the solution.

The fact that PEO does not appreciably interact with DPCl, which was confirmed both by ITC and NMR, is very important because it furnishes evidence that a certain amount of low molar mass PEO homopolymer in the studied sample does not appreciably affect the results and general conclusions concerning the electrostatic coassembly of the studied sample with cationic surfactant. It is true that the stabilizing PEO blocks are somewhat shorter than those calculated theoretically using information from the supplier, but they are long enough to secure a good solubility and long-time stability of investigated solutions. Low molar mass of PEO homopolymer admixtures does not almost affect the scattering data; due to their low contrast, they are practically invisible in microscopy imaging (as well as in SAXS and in SANS—measured earlier[18]) and as they do not interact with DPCl and they do not affect the association processes and structure of studied associates.

The most important finding concerns the rate of the studied self-assembly. Despite the fact that the intensity of the X-ray beam is high, which causes some degradation of studied complexes and precludes accurate kinetic measurements, the comparison of stopped-flow data with those from a long-time equilibrated system shows that the formation of structured insoluble domains is very fast (<50 ms). The comparison also suggests that the structure development contains at least two time steps differing in rates: (i) fast initial step (<50 ms) and (ii) slower "aging" or "relaxation" process proceeding on the 10^{-1}−10^{0} s time scale.

■ ASSOCIATED CONTENT

Ⓢ Supporting Information

Detailed analysis of the sample used; ITC study of the micellization of pure DPCl surfactant. This material is available free of charge via the Internet at http://pubs.acs.org.

■ AUTHOR INFORMATION

Corresponding Author

*E-mail: mariuszuchman@go2.pl.

Notes

The authors declare no competing financial interest.

■ ACKNOWLEDGMENTS

The authors acknowledge the financial support from the Ministry of Education of the Czech Republic (long-term Research Project MSM0021620857) and the Grant Agency of the Czech Republic (Grants P208/10/0353, P208/12/P236, P205/11/J043, and P106/12/0143) and German Academic Exchange Service DAAD (Grants 2B08021 and D0804221 PPP-CZ-09-10, PKZ: 50016729). T.C. ackowledges the support from NRF (2012K2A1A6047736). M.U. thanks Gerd Olofsson for discussions on ITC during ECIS 2012 and Ingo Hoffmann for the assistance with ITC measurements at TU Berlin.

■ REFERENCES

(1) Harada, A.; Kataoka, K. *Macromolecules* **1995**, *28*, 5294.
(2) Kabanov, A. V.; Bronich, T. K.; Kabanov, V. A.; Yu, K.; Eisenberg, A. *Macromolecules* **1996**, *29*, 6797.
(3) Berret, J.-F. *Adv. Colloid Interface Sci.* **2011**, *167*, 38.
(4) Kogej, K. *Adv. Colloid Interface Sci.* **2010**, *158*, 68.
(5) Langevin, D. *Adv. Colloid Interface Sci.* **2009**, *147*−*148*, 170.
(6) Voets, I. K.; de Keizer, A.; Stuart, M. A. C. *Adv. Colloid Interface Sci.* **2009**, *147*−*148*, 300.
(7) Tam, K. C.; Wyn-Jones, E. *Chem. Soc. Rev.* **2006**, *35*, 693.
(8) Dobrynin, A. V.; Rubinstein, M. *Prog. Polym. Sci.* **2005**, *30*, 1049.
(9) Pispas, S. *Soft Matter* **2011**, *7*, 8697.
(10) Pergushov, D. V.; Borisov, O. V.; Zezin, A. B.; Muller, A. H. E *Adv. Polym. Sci.* **2011**, *241*, 131.
(11) Burkhardt, M.; Ruppel, M.; Tea, S.; Drechsler, M.; Schweins, R.; Pergushov, D. V.; Gradzielski, M.; Zezin, A. B.; Muller, A. H. E. *Langmuir* **2008**, *24*, 1769.
(12) Bronich, T. K.; Kabanov, A. V.; Kabanov, V. A.; Yu, K.; Eisenberg, A. *Macromolecules* **1997**, *30*, 3519.
(13) Kabanov, A. V.; Bronich, T. K.; Kabanov, V. A.; Yu, K.; Eisenberg, A. *J. Am. Chem. Soc.* **1998**, *120*, 9941.
(14) Bronich, T. K.; Popov, A. M.; Eisenberg, A.; Kabanov, V. A.; Kabanov, A. V. *Langmuir* **2000**, *16*, 481.
(15) Hoffmann, I.; Heunemann, P.; Prévost, S.; Schweins, R.; Wagner, N. J.; Gradzielski, M. *Langmuir* **2011**, *27*, 4386.
(16) Berret, J.-F.; Vigolo, B.; Eng, R.; Hervé, P.; Grillo, I.; Yang, L. *Macromolecules* **2004**, *37*, 4922.
(17) Mironov, A. V.; Starodoubtsev, S. R.; Khokhlov, A. R.; Dembo, A. T.; Yakunin, A. N. *Macromolecules* **1998**, *31*, 7698.
(18) Uchman, M.; Štěpánek, M.; Prévost, S.; Angelov, B.; Bednár, J.; Appavou, M.-S.; Gradzielski, M.; Procházka, K. *Macromolecules* **2012**, *45*, 6471.
(19) Matejicek, P.; Štěpánek, M.; Uchman, M.; Procházka, K.; Spirkova, M. *Collect. Czech. Chem. Commun.* **2006**, *71*, 723.
(20) Thalberg, K.; Lindman, B.; Bergfeldt, K. *Langmuir* **1991**, *7*, 2893.
(21) Wang, X.; Li, Y.; Li, J.; Wang, J.; Wang, Y.; Guo, Z.; Yan, H. *J. Phys. Chem. B* **2005**, *109*, 10807.
(22) Mezei, A.; Ábrahám, A.; Pojjak, K.; Meszaros, R. *Langmuir* **2009**, *25*, 7304.
(23) Pojjak, K.; Bertalanits, E.; Meszaros, R. *Langmuir* **2011**, *27*, 9139.
(24) Matsuda, T.; Annaka, M. *Langmuir* **2008**, *24*, 5707.
(25) Wang, C.; Tam, K. C. *J. Phys. Chem. B* **2003**, *107*, 4667.
(26) Jerschow, A.; Müller, N. *J. Magn. Reson.* **1997**, *125*, 327.
(27) Johnson, C. S. *Prog. Nucl. Magn. Reson. Spectrosc.* **1999**, *34*, 203.
(28) Longsworth, L. G. *J. Phys. Chem.* **1960**, *64*, 1914.
(29) Panine, P.; Finet, S.; Weiss, T. M.; Narayanan, T. *Adv. Colloid Interface Sci.* **2006**, *127*, 9.
(30) Trap, H. J. L.; Hermans, J. J. *J. Phys. Chem.* **1954**, *58*, 757.
(31) Stepanek, M.; Podhajecka, K.; Tesarova, E.; Prochazka, K.; Tuzar, Z.; Brown, W. *Langmuir* **2001**, *17*, 4240.
(32) Podhajecka, K.; Stepanek, M.; Prochazka, K.; Brown, W. *Langmuir* **2001**, *17*, 4245.
(33) Mehrian, T.; de Keizer, A.; Korteweg, A. J.; Lyklema, J. *Colloids Surf., A* **1993**, *71*, 255.
(34) Korotkikh, O. P.; Kochurova, N. N. *Russ. J. Appl. Chem.* **2006**, *79*, 1204.
(35) Olofsson, G.; Loh, W. *J. Braz. Chem. Soc.* **2009**, *20*, 577.
(36) Courtois, J.; Berret, J.-F. *Langmuir* **2010**, *26*, 11750.
(37) Rigsbee, D. R.; Dubin, P. L. *Langmuir* **1996**, *12*, 1928.
(38) Zheng, P.; An, X.; Peng, X.; Shen, W. *J. Phys. Chem. B* **2009**, *113*, 13566.
(39) Bai, G.; Wang, Y.; Yan, H.; Thomas, R. K.; Kwak, J. C. T. *J. Phys. Chem. B* **2002**, *106*, 2153.
(40) Wang, C.; Tam, K. C. *J. Phys. Chem. B* **2004**, *108*, 8976.
(41) Wang, C.; Tam, K. C. *Langmuir* **2002**, *18*, 6484.
(42) Dastidar, S. G.; Mukhopadhyay, C. *Phys. Rev. E: Stat., Nonlinear, Soft Matter Phys.* **2004**, *70*, 061901.
(43) Lodge, T. P.; Bang, J.; Hanley, K. J.; Krocak, J.; Dahlquist, S.; Sujan, B.; Ott, J. *Langmuir* **2003**, *19*, 2103.
(44) Lad, M. D.; Ledger, V. M.; Briggs, B.; Green, R. J.; Frazier, R. A. *Langmuir* **2003**, *19*, 5098.
(45) Matejicek, P.; Brus, J.; Jigounov, A.; Plestil, J.; Uchman, M.; Prochazka, K.; Gradzielski, M. *Macromolecules* **2011**, *44*, 3847.
(46) Patel, M. M.; Anchordoquy, T. J. *Biophys. J.* **2005**, *88*, 2089.
(47) Marcus, Y. *Pure Appl. Chem.* **2010**, *82*, 1889−1899.
(48) Humpolickova, J.; Stepanek, M.; Prochazka, K.; Hof, M. *J. Phys. Chem. A* **2005**, *109*, 10803.
(49) Hunter, R. J. *Foundations of Colloid Science*; Oxford University Press: New York, 2001; pp 438−443.
(50) Sandt, Ch.; Barbeau, J.; Gagnon, M.-A.; Lafleur, M. *J. Antimicrob. Chemother.* **2007**, *60*, 1281.
(51) Lund, R.; Willner, L.; Pipich, V.; Grillo, I.; Lindner, P.; Colmenero, J.; Richter, D. *Macromolecules* **2011**, *44*, 6145.
(52) Meli, L.; Santiago, J. M.; Lodge, T. P. *Macromolecules* **2010**, *43*, 2018.
(53) Aniansson, E. A. G.; Wall, S. N.; Almgren, M.; Hoffman, H.; Kielmann, I.; Ulbricht, W.; Zana, R.; Lang, J.; Tondre, C. *J. Phys. Chem.* **1976**, *80*, 905.
(54) Aniansson, E. A. G.; Wall, S. N. *J. Phys. Chem.* **1974**, *78*, 1024.
(55) Riess, G. *Prog. Polym. Sci.* **2003**, *28*, 1107.
(56) Munk, P. In *Solvents and Self-Organization of Polymers*; Webber, S. E., Munk, P., Tuzar, Z., Eds.; Kluwer Academic Publisher: Dordrecht, 1996; pp 19−33.
(57) Bednar, B.; Edwards, K.; Almgren, M.; Tormod, S.; Tuzar, Z. *Makromol. Chem., Rapid Commun.* **1998**, *9*, 785.
(58) Pacovska, M.; Prochazka, K.; Tuzar, Z.; Munk, P. *Polymer* **1993**, *34*, 4585.
(59) Prochazka, K.; Vajda, S.; Fidler, V.; Bednar, B.; Mukhtar, E.; Almgren, M.; Holmes, S. *J. Mol. Struct.* **1990**, *219*, 377.